Homogenized daily sunshine duration over China from 1961 to 2022

Yanyi He[1,3], Kaicun Wang[2*], Kun Yang[3], Chunlüe Zhou[1*], Changkun Shao[3], and Changjian Yin[2]

[1] School of Geography and Planning, Sun Yat-sen University, 510275 Guangzhou, China

[2] Institute of Carbon Neutrality, Sino-French Institute for Earth System Science, College of Urban and Environmental Sciences, Peking University, 100081 Beijing, China

[3] Department of Earth System Science, Ministry of Education Key Laboratory for Earth System Modeling, Institute for Global Change Studies, Tsinghua University, 100084 Beijing, China

[*]**Corresponding Author:** Kaicun Wang, kcwang@pku.edu.cn; Chunlüe Zhou, zhouchunlue@mail.sysu.edu.cn

Earth System Science Data

Date submitted: October 24, 2024

Date submitted: February 11, 2025

Abstract

Inhomogeneities in the sunshine duration (SSD) observational series, caused by non-climatic factors like China's widespread transition from manual to automatic SSD recorders in 2019 or station relocations, have hindered accurate estimate of near-surface solar radiation. These issues significantly affect ~~for~~ the analysis of global dimming and brightening as well as related applications, such as solar energy planning and agriculture management. This study compiled raw SSD observational data from 1961 to 2022 at more than 2,200 stations in China and clearly found that the improved precision from 0.1 hour to 1 minute following the instrument update in 2019 led to a sudden reduction in the frequency of zero SSD from 2019 onwards, referred to as the day0-type discontinuity. For the first time, we systematically corrected this known day0-type discontinuity at 378 stations (17%) in China, resulting in an SSD series with comparable frequencies of zero value before and after 2019. On this base, we constructed a homogenization procedure to detect and adjust discontinuities in both the variance and mean of daily SSD from 1961 to 2022. Results show that a total of 1,363 (60%) stations experienced breakpoints in SSD, of which ~65% were confirmed by station relocations and instrument replacements. Compared to the raw SSD, the homogenized SSD is more continuous to the naked eye for various periods, and presents weakened dimming ($p<0.05$) across China from 1961 to 1990 but a non-significant positive trend by a reduction of 60% in the Tibetan Plateau, suggesting that the homogenized SSD tends to better capture the dimming phenomenon. The northern regions continue dimming from 1991 to 2022 but the southern regions of China brighten slightly. The implementation of the Action Plan for Air Pollution Prevention and Control since 2013 has contributed to a reversal of SSD trend thereafter, which is better reflected in the homogenized SSD with a trend shift from -0.02 to 0.07 hours·day^{-1}/decade from 2013 to 2022 in China, especially in heavily polluted regions. Besides, the relationships of cloud cover fraction and aerosol optical depth with SSD are intensified in the homogenized dataset. These results highlight the importance of the homogenized SSD in accurately understanding the dimming and brightening phenomena. The homogenized SSD dataset is publicly available for community use at https://doi.org/10.11888/Atmos.tpdc.301478 (He et al., 2024).

Formatted: Font: Italic

1. Introduction

Sunshine duration (SSD) is one of the indispensable observation indicators in ground-based meteorological measurements. It, capturesing the duration of direct sunlight reaching the Earth's surface (Wild et al., 2009; He et al., 2018). As an essential reference indicator to explore variations in surface incident solar radiation (R_s), SSD has profound implications for monitoring climate change, weather forecasting, ecosystem management, and solar energy generation (Stanhill and Cohen, 2003; Baumgartner et al., 2018). Therefore, making high-quality homogenized SSD data publicly accessible to diverse industries is crucial for research, decision-making, and planning across various sectors.

SSD measurement dates back 170 years ago, when the sum of sub-periods for which direct solar radiation exceeds 120 W/m^2 was defined as SSD (WMO, 2014). SSD measurements can be broadly categorized into manual and automatic SSD recorders according to the need of human supervision (Wang et al., 2021). The commonly used manual SSD recorders include the Campbell-Stokes sunshine recorder and the Jordan sunshine recorder (Baumgartner et al., 2018). These instruments operate by focusing direct solar radiation onto the photosensitized paper, which burns and leaves one or more continuous traces that represents one or multiple subperiods of sunshine duration (Che et al., 2005; Zhao et al., 2010). SSD is calculated as the sum of the subperiods of the burn within a calendar day. Automatic sunshine recorders employ sensors for observations and the types are diverse, including pyrheliometer, pyranometer, photovoltaic sunshine recorders, and more (Lv et al., 2015).

Since the 1950s, the Jordan sunshine recorder has been the primary instrument for measuring SSD in most meteorological stations in China. As reported, only 18 stations in the Heilongjiang Province of Northeast China utilized the Campbell-Stokes sunshine recorder that was subsequently replaced by the Jordan sunshine recorder in 2012 (Lu et al., 2012). In 2019, China carried out a widespread replacement of the Jordon sunshine recorders transitioning to the photoelectric digital SSD recorders at more than 2,400 stations to achieve the automation of SSD measurement (Wang et al., 2020). In the first half of 2019, parallel observations were conducted using both instruments, but starting from the second half of the year, only automatic sunshine recorders were used to record SSD. Compared to traditional manual methods,

automatic sunshine recorders have higher precision and automation (Wang et al., 2020).

Recent studies have compared parallel observations for the two measurements at some stations for certain regions of China (Lv et al., 2015; Hu et al., 2019; Lu et al., 2019; Lang et al., 2021; Zhou et al., 2021b; Dai et al., 2022). They reported a relatively strong consistency between both observations, but a certain degree of discrepancies still remain, which is closely tied to the position of the sun and varying weather conditions: 1) the photoelectric digital recorders tend to record higher values during weak direct radiation at sunrise and sunset and lower values during strong noon radiation, compared to manual observations; and 2) under persistently sunny weather, the more sensitive photoelectric digital recorders have slightly longer SSD than the manual recorders, but the manual recorders under cloudy conditions with intermittent sunshine tend to register artificially higher values due to lower instrument accuracy and the spot effect.

Manual sunshine recorders ~~Despite~~ do not suffer from~~the absence of~~ a sensitivity drift issue in SSD observations~~ by manual sunshine recorders~~, attributed to the daily replacement of photosensitized paper (Sanchez-Lorenzo and Wild, 2012).~~,~~ However, the consistency of observational data still faces a challenge~~s in ensuring consistency~~ due to the subjectivity introduced by different observers in practice. On the other hand, due to the limitations of current observation technology, the photoelectric digital SSD recorders also have shortcomings, such as narrow spectral response range, high sensitivity to nearby environment, complex instrument maintenance, and instrument sensitivity drift and difficulty in calibration (Wang et al., 2015; Wang et al., 2021). Several studies have confirmed that the replacement of instruments can lead to non-climatic shifts in SSD and also applied a homogenization to SSD in Iberian Peninsula (Sanchez-Lorenzo et al., 2007), Switzerland (Sanchez-Lorenzo and Wild, 2012), Italy (Manara et al., 2015), and Japan (Ma et al., 2022). Besides, other non-climatic factors such as station relocations could also introduce some systematic errors in SSD.

~~Taking into account~~Given the aforementioned issues in SSD observations, it is imperative to detect and adjust the discontinuities of SSD series in China, especially in the presence of artificial errors caused by changes in observing instruments, station locations, nearby environmental conditions, observing procedures, or other factors. To achieve this, this study

compiled raw SSD data and systematically corrected the known day0-type discontinuity, as described in Section 2.1-2.2. In Section 2.3, a homogenization procedure was described to detect and adjust series discontinuities in the variance and mean of daily SSD, with establishing a reliable reference series. Section 3.1-3.2 analyzed the detected breakpoints and assessed the impacts of series homogenization on trends across various periods. We further examined the influence of cloud cover and aerosols on SSD variations in China in Section 3.3. This study produced a 62-year (1961-2022) homogenized daily SSD dataset in China, which are publicly accessible. The dataset can be used to support research on China's dimming and brightening phenomena, to improve the assessment of solar radiation simulations and future projections, and to provide valuable data for various applications such as solar energy layout.

2. Data and methods

2.1 Data

The daily observed SSD at 2,425 meteorological stations from 1961 to 2022 were collected from the China Meteorological Administration (CMA, http://data.cma.cn/en/). After screening stations based on data continuity and length, i.e., ≥15 days of data per month, ≥10 months per year, and ≥50 years during the entire period, a total of 2,263 stations were involved in this study. Again, a widespread replacement of instruments across China occurred around 2019, transitioning from dark-tube sunshine recorder to photoelectric digital sunshine recorder (Wang et al., 2020).

R_s is highly correlated with SSD, but serious concerns have been raised about the reliability of observational R_s data due to poor spatial representativeness, temporal discontinuity, and the effects of urbanization (Wild et al., 2005; Wang et al., 2014; He et al., 2018). In particular for China, issues related to instrument aging, sensitivity drift, and instrument replacements have notably contributed to spurious variations in R_s observations at ~100 stations (He and Wang, 2020). Therefore, R_s series from nearby stations are insufficient to serve as reference series during homogenization due to their sparse distribution and data inhomogeneity. Reanalysis products have dynamically consistent and spatiotemporally complete atmospheric fields with

high resolution and open access of data, addressing these limitations of R_s observations (Zhou et al., 2017). Among these reanalysis products, ERA5 has been verified to outperform in R_s simulations across hourly, daily, monthly, interannual, and decadal scales in China (He et al., 2021; Li et al., 2023). Leveraging the ERA5 R_s data (https://cds.climate.copernicus.eu/cdsapp#!/dataset/reanalysis-era5-single-levels), we estimated sunshine duration based on the criteria of hourly direct R_s exceeding 120 W/m² that is consistent with instrument measurements (He et al., 2018), to serve as a reference series for homogenizing the observational SSD data. Meanwhile, SSD estimate from hourly direct R_s of MERRA2 data from 1980 to 2022 (https://gmao.gsfc.nasa.gov/reanalysis/MERRA-2/) was used as an aid in constructing the reference series.

To examine the effects of cloud and aerosol on SSD variations, daily cloud cover fraction (CCF) and aerosol optical depth at 550nm (AOD) from 2003 to 2022 were obtained from a MODIS product at 1°×1° grids (MCD06COSP_D3, https://ladsweb.modaps.eosdis.nasa.gov/archive/allData/62/MCD06COSP_D3_MODIS) (Pincus et al., 2012; Swales et al., 2018). Cloud cover fraction is calculated as the percentage of a grid cell that is covered by clouds, with values ranging from 0 (no clouds) to 1 (completely overcast). AOD at 550nm is a measure of the total aerosol content in the atmosphere, quantifying how much sunlight is absorbed and scattered by aerosols, with values ranging from 0 (no aerosol) to values greater than 1 (high aerosol loading).

According to topography and administrative divisions in China, seven subregions were identified as shown in Figure 1a, i.e., Northwest China (I), the Tibetan Plateau (II), Southwest China (III), Northeast China (IV), North China (V), Southeast China (VI), and the Loess Plateau (VII). A relocation event of station was defined as Δlatitude > 0.01°, Δlongitude > 0.01°, or Δaltitude > 10m before and after a specific date. The history of station relocations in China is reflected by the number of relocations in Figure 1a, and the fraction of the stations with relocations from 1961 to 2022 in Figure 1b. The average of the number of relocations in China is about 4 (Fig. 1a). The instrument replacements in 2019 are accompanied with changes of the measurement height, presenting the unusually frequent relocations at the time (Fig. 1b).

2.2 Correction of known day0-type discontinuity

Following the update of automatic sunshine recorders around 2019, which improved measurement precision from 0.1 hour to 1 minute (Lang et al., 2021), we observed a sudden reduction in the frequency of zero SSD at specific stations in China after 2019. In most instances, raw daily SSD is absent of a value of zero for more than six consecutive months, which is significantly different from series pattern observed prior to 2019. We identified the segments with this known day0-type discontinuity that characterized by more than six consecutive months of non-zero SSD.

Results show that the day0-type discontinuity occurs almost in one segment per station, totaling 378 stations (i.e., 17% of stations in China) distributed mainly across northern China, Tibetan Plateau, and part of Southwest China (Fig. 2a), and is concentrated in 2019 to 2020 (Fig. 2b). Note that the improved precision may not lead to a notable day0-type discontinuity in some regions or such minor discontinuities may not be easily identifiable. The spatial distribution of discontinuities and the years of their most frequent occurrence align with the update of automatic sunshine recorders in 2019 or later, as well as with station relocations (Figs. 1 vs 2). We employed the quantile-matching (QM) algorithm to correct the segments with the identified day0-type discontinuities by utilizing the longest segment that is free of the discontinuity, which produced the SSD0 series for the subsequent homogenization. The magnitude of correction reaches up to -5 hours·day^{-1} at two example stations in Northeast China and Northwest China, respectively (Fig. 3a and 3d). After correction, the frequency of low values, especially zero values, has increased visibly in 2019 or later in the SSD0 series compared to the raw SSD series, and then is comparable to the frequency before 2019 (Fig. 3b and 3e). The monthly SSD0 anomaly after correction appears to be more continuous (Fig. 3c and 3f). Note that the mean shift of the segment after 2020 like at station No. 51627 (Fig. 3f) would be statistically homogenized in the following sections.

2.3 Homogenization procedure

Since parallel observations for the photoelectric digital SSD recorder and manual SSD recorder are not publicly available, we are unable to directly explore the relationship between

the two datasets. Data series homogenization offers us with an effective way to address discontinuities in climate time series caused by non-climatic factors like station relocation and instrument replacements. Much effort has been devoted to develop homogenization methods, such as the standard normal homogeneity test (SNHT) (Alexandersson, 1986), two-phase regression-based methods (Solow, 1987), Bayesian-based methods (Perreault et al., 2000; Chu and Zhao, 2004), penalized maximal *T* test (PMT) (Wang et al., 2007), and penalized maximal *F* test (PMF) (Wang, 2008a). Reeves et al. (2007) compared these methods and argued that SNH test may work best when trend and periodic effects are diminished by using homogeneous reference series. However, Wang et al. (2007) and Wang (2008a) pointed out that unequal sample sizes affect the false alarm rate and detection power of SNHT-type tests.

They demonstrated that PMT and PMF tests with incorporating penalized empirical corrections offer higher detection power and are suited for long-term series with significant climate trends (Wang, 2008b; Wang et al., 2010). The PMT test searches for the most likely location of mean shifts in segments of the difference between the candidate and reference series using a recursive testing algorithm (Wang et al., 2007). The PMF test, on the other hand, detects undocumented mean shifts in the difference series with a linear trend by employing a common-trend two-phase regression model (Wang, 2008a). Both test algorithms account for the lag-1 autocorrelation of the series. Since their release, PMT and PMF tests have been successfully applied to various climate elements including temperature, precipitation, humidity, wind speed, and R_s (Wang et al., 2010; Dai et al., 2011; Domonkos, 2011; Yang et al., 2018; Zhou et al., 2018; Ma et al., 2022; Zhou et al., 2022), making them the chosen methods for this study. For variance shifts in the series, an improved Kolmogorov–Smirnov (K-S) test has been widely used to assess whether two samples follow similar or different distributions (Press et al. 1992). To account for the effects of the lag-1 autocorrelation and sample size, Dai et al. (2011) and Zhou et al. (2021a) developed critical values for certain significance levels through a series of Monte Carlo simulations.

Formatted: Not Highlight

During the homogenization, a well-established reference series is essential for sufficiently detecting and adjusting inhomogeneities in long-term climate time series., ~~s~~ Because~~ince~~ it ~~can~~

helps remove most real climate changes and synoptic variations (i.e., noise), ~~thereby improving~~ enhancing the signal-to-noise ratio of discontinuities and enabling statistical detection and removal of spurious shifts (Dai et al., 2011; Zhou et al., 2022). In this study, we first established a reliable reference series to account for background weather and climate variations, and then detected and adjusted spurious breakpoints in the mean and variance of the non-zero daily SSD0 series using the well-established ERA5 reference series, resulting in a homogenized daily SSD observational dataset.

2.3.1 Construction of the reference series

A reliable reference series should effectively capture most background weather and climate variations while remaining homogeneous. ERA5 SSD series is highly correlated with the SSD0 series on daily and monthly time scales across China (Fig. 4a and 4d), which ensures that ERA5 SSD as a reference series can remove most background weather and climate variations from the SSD0 series, thereby facilitating the detection of breakpoints.

Previous studies have indicated that ERA5 significantly overestimates the variation in R_s from 2003 to 2010 in China (He et al., 2021; Shao et al., 2022). This overestimation is inherited in the SSD estimated from hourly direct R_s of ERA5, presenting inhomogeneities during this period, particular in North China and Southeast China (Fig. 5). We evaluated ~~several~~ multiple reanalysis products and found that the SSD estimated from hourly direct R_s of MERRA2 does not suffer from this issue (Fig. 5), maybe since MERRA2 assimilates space-based observations of aerosols and improves R_s simulations in China to some extent (Feng and Wang, 2021). Meanwhile, MERRA2 SSD is also highly correlated with the SSD0 series (Fig. 4b and 4e). To ~~mitigate~~ resolve the discontinuity of ERA5 SSD from 2003 to 2010, we took MERRA2 SSD as the reference series and applied the PMT test to detect breakpoints in the monthly ERA5 SSD series. After obtaining the breakpoints, we employed the QM algorithm to adjust discontinuities in the daily ERA5 SSD series, using the longest segment as the reference. Note that, to minimize potential uncertainties as much as possible arising from incorporating MERRA2 SSD, the detection and adjustment described above are strictly limited to the period of 2003-2010. Results show that the homogenized ERA5 SSD not only exhibits higher correlations with the SSD0 series on daily and monthly time scales (Fig. 4c and 4f), but also

greatly alleviated the overestimation from 2003 to 2010 (Fig. 5), which makes it a suitable reference series for the subsequent homogenization.

2.3.2 Detection and adjustment of breakpoints in non-zero daily SSD0 series

Zero values in a daily meteorological series should remain unaltered unless supported by evidence or reports of trace occurrence or changes in measuring precision (Wang et al., 2010). After the known day0-type discontinuity has been corrected in Section 2.2 above, the subsequent homogenization was performed on the variance and mean of non-zero daily SSD0 series. To achieve this, we decomposed the non-zero daily SSD0 series into two components: intramonthly and monthly.

Firstly, we applied an improved Kolmogorov–Smirnov (K-S) test (Dai et al., 2011; Zhou et al., 2021a) at a 99.9% significance level to the intramonthly component of the daily difference series ($DSSDd_{intra}$) for detecting breakpoints in the variance of the non-zero daily SSD0 series:

$$DSSDd_{intra} = SSDa_{obs} - \alpha \cdot SSDa_{ERA5} \quad (1)$$

$$SSDa_{obs} = SSDd_{obs} - SSDm_{obs} \quad (2)$$

$$SSDa_{ERA5} = SSDd_{ERA5} - SSDm_{ERA5} \quad (3)$$

where $SSDd_{obs}$ and $SSDd_{ERA5}$ are the non-zero daily values of SSD0 and homogenized ERA5 SSD; $SSDm_{obs}$ and $SSDm_{ERA5}$ are the monthly mean $SSDd_{obs}$ and $SSDd_{ERA5}$; $SSDa_{obs}$ and $SSDa_{ERA5}$ are the daily anomalies of $SSDd_{obs}$ and $SSDd_{ERA5}$, respectively; α is the linear regression coefficient of $SSDa_{obs}$ against $SSDa_{ERA5}$. α displays higher values in the Tibetan Plateau, Northwest China, and the Loess Plateau, while remaining around 1 in the other regions (Fig. 6a). Systematic biases in the reanalysis and the effect of the station-versus-grid discrepancies can be also greatly eliminated by the regression against the observation.

Secondly, we applied both PMT and PMF tests developed by Wang et al. (2007) and Wang (2008b) at a 99% significance level to detect breakpoints in the monthly mean of the non-zero SSD0 series. The breakpoints detected by both methods within one year were kept. In the PMT test, $SSDm_{ERA5}$ was taken as the input of reference series. Consistently, the monthly difference series (DSSDm) requested in the PMF test was constructed as follows:

$$DSSDm = SSDm_{obs} - \beta \cdot SSDm_{ERA5} \quad (4)$$

where β is liner regression coefficient between $SSDm_{obs}$ and $SSDm_{ERA5}$. β exhibits a similar pattern to α, showing high value in the northwest and low value in the southeast (Fig. 6b).

To obtain a manageable number of breakpoints in the final, we followed the approach of Zhou et al. (2021a) by setting 365 days between breakpoints as the threshold to merge the detected breakpoints above. For cases with three or more breakpoints within 365 days of each other, we retained only the middle breakpoint, and for two breakpoints, we kept the one with the larger test statistic.

Finally, we adopted the QM algorithm from Wang et al. (2010) to remove the merged breakpoints in the daily difference series (DSSDd) that is the residual series from the regression (the slope γ, Fig. 6c showing a relatively uniform pattern) of $SSDd_{obs}$ on $SSDd_{ERA5}$:

$$DSSDd = SSDd_{obs} - \gamma \cdot SSDd_{ERA5} \quad (5)$$

This produced a homogenized daily SSD dataset for China, covering the period from 1961 to 2022, with zero values backfilled. The longest segment was chosen as the baseline segment primarily due to its relative homogeneity and reliability. Despite the use of advanced automated instruments with higher precision from 2019 onwards, the segment is still too short to fully meet the criteria for a reliable baseline segment. The segment after 2019 will be considered as the baseline segment when the dataset is updated in the coming years.

3. Results

3.1 Detection and adjustment of breakpoints

One or two breakpoints in the variance of the $DSSDd_{intra}$ series were detected at 328 stations, mainly in Northwest China, Northeast China, North China, and the Loess Plateau (Fig. 7~~6~~a). Most of these breakpoints occur around 2019 (Fig. 7~~6~~a2), coinciding with the instrument replacements from dark-tube sunshine recorder to photoelectric digital sunshine recorder, as well as the station relocations (Fig. 1b). During the period of 1961-2022, 1,238 stations (55%) in China suffered from the breakpoints in the mean of the DSSDm series (Fig. 7~~6~~b1). These

breakpoints are evenly distributed across China (Fig. ~~6~~7b1), with many occurring around 2019 and two additional small peaks around 1972 and 2003 (Fig. ~~6~~7b2). Approximately 52% of the stations in China were detected with one breakpoint, 32% with two breakpoints, 12% with three breakpoints, and few stations with more than four breakpoints (Fig. 7~~6~~b1). After merging the two types of breakpoints above, a total of 1,363 stations experienced breakpoints, accounting for approximately 60% of the stations in China (Fig. 7~~6~~c1). The merged breakpoints are densely concentrated in northern China, where approximately 71% of the stations are affected, with the highest density (74%) observed on the Loess Plateau, while approximately 47% of the stations are affected in southern China (Fig. 7~~6~~c1). A higher fraction of stations with breakpoints occurs around 2019 after merging (Fig. 7~~6~~c2).

The detected breakpoints may be associated with factors such as instrument replacements, station relocations, equipment malfunctions, operation errors, and other environment changes, any of which may contribute to data series inhomogeneity (Sanchez-Lorenzo and Wild, 2012; Wang et al., 2020). To empirically demonstrate it, we attempted to collect such types of information but were only able to compile a detailed set of information about station relocation. We found that over 50% of stations in 2019 were relocated (Fig. 1b), mostly because they needed to change their positions or heights due to instrument replacements or urbanization. The hit probability for matching detected breakpoints with stations relocations is approximately 65%. Since the date of a station relocation does not always align with the date of a statistically detected breakpoint, this value is calculated as the ratio of the number of breakpoints that have one or more relocations within one year of the breakpoint to the total number of breakpoints. Noted that the breakpoints may be caused by factors other than station relocations, while some station locations may not have resulted in any breakpoints, or certain breakpoints may not have emerged from the background weather or climate variations that was not easily detected by a statistical method.

To remove the artificial breakpoints detected above, the QM algorithm was implemented to achieve homogenization by aligning the empirical distributions of all segments. For examples, three breakpoints in the variance and mean of the SSD0 series were detected at Station No. 51627 (Fig. 8~~7~~). The first two breakpoints are associated with the station

relocations and the last breakpoints are related to the replacement of instrument in 2019. The adjustments estimated based on the QM algorithm for the three breakpoints are approximately 1, -0.5, and 2.8 hours·day^{-1}, respectively (Fig. ~~7~~8b). After adjustments, the monthly SSD0 anomaly series appears continuous and reasonable, particularly after 2019 (Fig. ~~8~~7c).

3.2 Comparison of trends before and after homogenization

The discontinuities hidden in the series are bound to affect the estimate of long-term trends of SSD. Fig. ~~8~~9 shows series comparisons among the raw SSD, SSD0, and homogenized SSD averaged over China and its seven subregions. The most significant adjustments are evident in 2019 or later, occurring across China (Fig. 9~~8~~). This is jointly resulted from two aspects: the high robustness of dark-tube sunshine recorder in measuring SSD before 2019, and the widespread switch to photoelectric digital sunshine recorder in 2019 that caused notable shifts compared to earlier period. Based on the periods of dimming and brightening in China revealed by prior researches (He et al., 2018; He and Wang, 2020), trend analysis was conducted for two major periods: 1961-1990 and 1991-2022.

During the period of 1961-1990, the homogenized SSD exhibits a significant downward trend of -0.11 hours·day^{-1}/decade (p<0.05) in China, compared to a slightly steeper decline of -0.13 hours·day^{-1}/decade (p<0.05) in the raw SSD (Figs. 9~~8~~-10~~9~~ and Table 1), though the difference between the two is not evident. After homogenization, the dimming of homogenized SSD weakens across China except the Tibetan Plateau, with the most pronounced weakening in North China by 0.04 hours·day^{-1}/decade compared to the raw SSD (Figs. 9~~8~~-10~~9~~ and Table 1). Meanwhile, the Tibetan Plateau shows a reduced and non-significant increase in the homogenized SSD (0.02 hours·day^{-1}/decade with a reduction of 60%, p>0.10) compared to the raw SSD (0.05 hours·day^{-1}/decade, p<0.10) during the dimming period of China (i.e., 1961 to 1990) (Figs. 9~~8~~-10~~9~~ and Table 1), suggesting that the homogenized SSD tends to better describe the dimming phenomenon.

During the period of 1991-2022, only the southern regions of China experienced slight brightening, whereas the northern regions continued dimming (Fig. ~~9~~10). The national average SSD trend of China remains unchanged before and after homogenization, with a decline of about -0.04 hours·day^{-1}/decade (p<0.10) (Table 1). However, the magnitudes of decadal trends

change significantly across various regions. In heavily polluted regions such as North China and the Loess Plateau, the degree of dimming diminishes in homogenized SSD. Specifically, the SSD trend decreases from -0.14 hours·day^{-1}/decade (p<0.05) to -0.12 hours·day^{-1}/decade (p<0.05) in North China, and from -0.11 hours·day^{-1}/decade (p<0.05) to -0.08 hours·day^{-1}/decade (p>0.10) in the Loess Plateau (Figs. 9~~8~~-10~~9~~ and Table 1). In addition, for the Tibetan Plateau and Northeast China, the SSD after homogenization presents a more pronounced decline compared to the raw data (Figs. ~~8~~9-10~~9~~ and Table 1).

In 2013, China issued and implemented the Air Pollution Prevention and Control Action Plan (APPCAP), to address severe air pollution and its associated health risks. The subsequent strengthening of air quality measures may have contributed to a reversal of SSD trend thereafter. During the period of 2013-2022, the national average SSD in China shifts from a decrease of -0.02 hours·day^{-1}/decade to an increase of 0.07 hours·day^{-1}/decade after homogenization, reflecting well the effect of the APPCAP implementation on the SSD trend reversal compared to earlier periods (Figs. 9~~8~~-10~~9~~ and Table 1). Especially for heavily polluted regions like North China, Southeast China, Loess Plateau, and Northeast China, the homogenized SSD shows more brightening after homogenization, with the most notable increase in North China where the trend increases from 0.16 (p>0.10) to 0.42 (p<0.10) hours·day^{-1}/decade (Figs. 9~~8~~-10~~9~~ and Table 1). Due to the instrument replacement in 2019, the artificial breakpoints in the SSD series have been removed and the homogenized SSD series appear more continuous to the naked eye (Fig. 9~~8~~b-9~~8~~c). Specifically, the homogenized SSD has a weakened trend (-0.16 hours·day^{-1}/decade, p>0.10) compared to the raw data (-0.52 hours·day^{-1}/decade, p<0.05) in Northwest China. The homogenized SSD declines with -0.36 hours·day^{-1}/decade (p<0.10) and -0.16 hours·day^{-1}/decade (p>0.10) in the Tibetan Plateau and Southwest China, respectively (Fig. 9~~8~~b-9d). In summary, considering the uncertainties brought by ~~the~~ series inhomogeneities caused by non-climatic factors such as instrument replacements and station relocations, ~~it is very necessary to~~ address~~ing~~ these inhomogeneities is so necessary, particularly in studies focused on detecting and attributing global diming and brightening.

3.3 Relationships of cloud and aerosol with sunshine duration

Cloud and aerosol affect the amount of solar radiation reaching the Earth's surface through sunlight reflection, absorption, and scattering, making their combined effects on solar radiation a key factor in understanding global dimming and brightening (Wild, 2009; Wild, 2012; Feng and Wang, 2021; Ma et al., 2022). SSD serves as a core indicator of solar radiation, which is modulated by both cloud cover and aerosols. Due to limitations of satellite data, this section focuses on the relationships of cloud cover fraction (CCF) and aerosol optical depth (AOD) on SSD variations solely over the 20-year period starting from 2003.

Fig. 1~~0~~ shows maps of decadal changes in AOD, CCF, and the homogenized SSD, and their time series at the locations collocated with stations in China. For the entire period of 2003-2022, the correlation coefficient of the averaged CCF in China against the raw SSD is -0.53 (p<0.05), and its coefficient against the homogenized SSD reaches -0.71 (p<0.05). On the other hand, in the heavily polluted regions such as North China and Northeast China, the correlation coefficient between AOD and SSD is significantly negative, and the relationships are intensified after homogenization, i.e., from -0.40 (p<0.10) to -0.56 (p<0.05) and from -0.41 (p<0.10) to -0.54 (p<0.10), respectively. These relationship changes indicate a stronger relationship with CCF and AOD in the homogenized SSD dataset.

During the period of 2003-2012, the average SSD in China decreases at a rate of -0.20 hours·day^{-1}/decade (p>0.10), accompanied by slight increases in both CCF and AOD (Fig. 1~~0~~g). For regional details, the significant increase of AOD in North China (Fig. ~~10a~~11a) and the significant increase in CCF in Southeast China (Fig. ~~10b~~11b) jointly contributes to regional divergences in the SSD decadal changes of China during this period (Fig. 1~~0~~c).

The effect of the APPCAP implementation on AOD can be clearly seen with a rapid reduction after 2013 (Fig. 1~~0~~a, 1~~0~~d, and 1~~0~~g). CCF also exhibits a corresponding shift from the perspective of spatial distribution of its decadal changes, especially in North China (Fig. 1~~0~~b vs 1~~0~~e), maybe due to various cloud-aerosol interactions. These changes of AOD and CCF contributes to the SSD brightening after 2013, which is reflected in the maps and time series of their decadal changes (Fig. 1~~0~~). During the period of 2013-2022, the spatially coherent pattern of AOD decadal reductions (-0.12 1/decade, p<0.05) inevitably lead to an

overall SSD brightening, on the basis of which the spatial detail of CCF decadal changes further inversely shapes the pattern of SSD decadal changes (Fig. 1~~0~~d-1~~0~~f). This results in a decadal change of 0.07 hours·day^{-1}/decade (p>0.10) in the national average SSD (Fig. 1~~0~~g). In heavily polluted regions such as North China, it's clear that decreases in both AOD and CCF jointly result in the enhanced brightening in the localized SSD (Fig. 1~~0~~d-1~~0~~f).

4. Data availability

The homogenized dataset of daily sunshine duration at 2.0×2.0 grids in China from 1961 to 2022 generated in this study, provides a valuable database for assessing and attributing solar radiation variations. It will~~, and will~~ also be a key for various applications in the solar energy industry, agricultural management, and ecology and climatology research. The homogenized dataset is freely accessed via the following link, https://doi.org/10.11888/Atmos.tpdc.301478 (He et al., 2024).

5. Conclusions and discussion

Inhomogeneities in climate series, stemming from non-climatic factors such as instrument replacements and station relocations, inevitably affect the estimate of long-term trends. While dark-tube sunshine recorder robustly measured SSD in China prior to 2019, the widespread transition to photoelectric digital sunshine recorder in 2019 introduced significant non-climate discontinuities in SSD. After compiling raw SSD observational data, we first noted a sudden reduction in the frequency of zero SSD in segments from 2019 onwards, attributed to improved measurement precision from 0.1 hour to 1 minute following the instrument update in 2019. This known day0-type discontinuity affected a total of 378 stations (~17% of stations in China), occurring almost in one segment per station, predominantly located in northern China, the Tibetan Plateau, and parts of Southwest China. We applied the quantile-matching algorithm to correct the segments with the day0-type discontinuities, using the longest segment unaffected by the discontinuity, which produced the SSD0 series that has comparable frequencies of zero SSD before and after 2019.

To further address the remaining discontinuities, we developed a homogenization procedure for producing a 62-year (1961-2022) homogenized daily SSD dataset in China. First, a well-established ERA5 SSD was constructed as a reliable reference series with the help of MERRA2 SSD to eliminate the background weather and climate variations (i.e., noise) for enhancing the signal-to-noise of artificial discontinuities. Second, two separate steps were taken to statistically detect discontinuities in the variance and mean of the non-zero daily SSD0 series. Results show that breakpoints in the variance are mainly concentrated in the northern part of China, while the breakpoints in the mean are evenly distributed across China. After merging the two types of breakpoints above, a total of 1,363 stations experienced breakpoints, accounting for ~60% of the stations in China. The peak in the number of breakpoints occurs in 2019, coinciding with the nationwide transition from manual to automated SSD recorders. In all, ~65% of the detected breakpoints were confirmed by station relocations and associated instrument replacements. Finally, the merged breakpoints were removed by the quantile-matching algorithm to produce the final homogenized daily dataset.

Compared to the raw SSD, the homogenized SSD shows more continuous variations across various time scales, providing a solid basis for estimating reliable long-term trends for various periods. During the dimming (1961 to 1990), the homogenized SSD presents weakened dimming across China compared to the raw SSD, and shows ~~particularly in the Tibetan Plateau, where the~~a trend shift~~s~~ in the Tibetan Plateau from a significantly positive to a non-significant ~~negative~~ positive with a reduction of 60%, suggesting that the homogenized SSD tends to better describe the dimming phenomenon. Xia (2010) reported a homogenized SSD trend in China during this period that is consistent with our result, but did not address the day0-type discontinuity issue and only limited the analysis to 2005. The future use of the homogenized SSD in solar radiation estimation could better correct the spurious largest dimming trend in China during this period revealed by low-quality ground-based observation of solar radiation (Wild, 2012; He et al., 2018; Tang et al., 2023).– During the period of 1991-2022, only the southern regions of China experienced slight brightening, whereas the northern regions continued dimming. In heavily polluted regions such as North China and the Loess Plateau, the extent of dimming diminishes in homogenized SSD. The subsequent strengthening of air

quality measures after issuing the APPCAP in 2013 in China may have contributed to a reversal of SSD trend thereafter. During the period of 2013-2022, the national average SSD in China shifts from a decrease of -0.02 hours·day^{-1}/decade to an increase of 0.07 hours·day^{-1}/decade after homogenization, reflecting well the effect of the APPCAP implementation on the SSD trend reversal compared to earlier periods. Especially in heavily polluted regions, the homogenized SSD shows more brightening after homogenization, with the most notable increase observed in North China.

We further examined the regulatory effects of clouds and aerosols on SSD changes using the satellite data from 2003 to 2022. Our analysis reveals that the relationships of CCF and AOD with SSD are intensified in the homogenized dataset. During the period of 2003-2012, the average SSD in China decreases at a rate of -0.20 hours·day^{-1}/decade (p>0.10), accompanied by slight increases in both CCF and AOD. The effect of the APPCAP implementation on AOD is evident, with a rapid reduction in AOD after 2013. In the subsequent period from 2013 to 2022, the spatially coherent pattern of AOD decadal reductions results in an overall SSD brightening, on the basis of which the spatial detail of CCF decadal changes further inversely shapes the pattern of SSD decadal changes. This leads to a national average SSD change of 0.07 hours·day^{-1}/decade (p>0.10). These regulatory effects of clouds and aerosols on SSD obtained using only 20-years satellite CCF and AOD data were also confirmed by prior studies regarding R_s. For instances, earlier studies have demonstrated that clouds were only able to explain R_s changes in the southern part of China before 1990, but accounted for changes across the entire China after 1990 (Yang et al., 2013; He and Wang, 2020). Wang et al. (2012) suggested that seasonal and interannual variations in R_s are predominantly affected by clouds, while decadal variations are mainly dominated by aerosols. It would be valuable to further investigate whether urbanization effect on SSD emerges after the APPCAP implementation in 2013 despite Wang et al. (2017) reporting no such effect before 2013.

Our long-term homogenized daily SSD dataset provides a solid database for various empirical and machine learning models to predict solar radiation (Fan et al., 2019). It not only

~~not only~~ enables ~~es~~ a reliable assessment of global dimming and brightening in China, but also provides~~es~~ valuable insights for planning, designing, and evaluating benefits across ~~various~~ multiple sectors, including solar energy, agriculture, and environmental management. Moreover, the homogenization experience including constructing a reference series with the aid of current atmospheric reanalysis could be adapted to have broader applications in the homogenization of other climate elements or over other regions to develop a global dataset.

Author contributions

YH, KW, and KY designed the research. YH performed the analysis and wrote the draft. CZ advised the homogenization method. KW and CY collected raw SSD observational data and YH compiled all the remaining data. All the authors jointly contributed to interpreting the results and editing the final paper.

Competing interests

The authors have declared no any competing interests.

Acknowledgements This study was supported by the National Natural Science Foundation of China (No. 42205171), the Starting Grant for Introduced Talents of Sun Yat-sen University (37000-12230039), and the Central University Basic Research Business Fee on the Training of Young Teachers (37000-31610006). Sunshine duration and other meteorological observations at 2,425 stations were obtained from the China Meteorological Administration (CMA, http://data.cma.cn/en). ERA5 and MEERA2 data were downloaded respectively at https://www.ecmwf.int/en/forecasts/datasets/reanalysis-datasets/era5 and https://gmao.gsfc.nasa.gov/reanalysis/MERRA-2/. MODIS data were downloaded at https://ladsweb.modaps.eosdis.nasa.gov/archive/allData/62/MCD06COSP_D3_MODIS.

References

Alexandersson, H.: A homogeneity test applied to precipitation data, J. Climatol., 6, 661-675, 1986.

Baumgartner, D., Pötzi, W., Freislich, H., Strutzmann, H., Veronig, A., Foelsche, U., and Rieder, H.: A comparison of long-term parallel measurements of sunshine duration obtained with a Campbell-Stokes sunshine recorder and two automated sunshine sensors, Theor. Appl. Climatol., 133, 263-275, 2018.

Che, H. Z., Shi, G. Y., Zhang, X. Y., Arimoto, R., Zhao, J. Q., Xu, L., Wang, B., and Chen, Z. H.: Analysis of 40 years of solar radiation data from China, 1961-2000, Geophys. Res. Lett., 32, 10.1029/2004gl022322, 2005.

Chu, P.-S. and Zhao, X.: Bayesian change-point analysis of tropical cyclone activity: The central North Pacific case, J. Clim., 17, 4893-4901, 2004.

Dai, A. G., Wang, J. H., Thorne, P. W., Parker, D. E., Haimberger, L., and Wang, X. L. L.: A New Approach to Homogenize Daily Radiosonde Humidity Data, J. Clim., 24, 965-991, 10.1175/2010JCLI3816.1, 2011.

Dai, H., Huang, S., Wang, Y., and Lai, L.: Analysis and evaluation based on parallel observation data of artificial and automatic sunshine observation in Jiangxi province, Jiangxi Science, 40, 370-373, 2022.

Domonkos, P.: Efficiency evaluation for detecting inhomogeneities by objective homogenisation methods, Theor. Appl. Climatol., 105, 455-467, 2011.

Fan, J., Wu, L., Zhang, F., Cai, H., Zeng, W., Wang, X., and Zou, H.: Empirical and machine learning models for predicting daily global solar radiation from sunshine duration: A review and case study in China, Renew. Sust. Energ. Rev., 100, 186-212, 2019.

Feng, F. and Wang, K. C.: Merging ground-based sunshine duration observations with satellite cloud and aerosol retrievals to produce high-resolution long-term surface solar radiation over China, Earth Syst. Sci. Data, 13, 907-922, 10.5194/essd-13-907-2021, 2021.

He, Y. and Wang, K.: Variability in direct and diffuse solar radiation across China from 1958 to 2017, Geophys. Res. Lett., 47, e2019GL084570, 10.1029/2019gl084570, 2020.

He, Y., Wang, K., and Feng, F.: Improvement of ERA5 over ERA-Interim in simulating surface incident solar radiation throughout China, J. Clim., 34, 3853–3867, 2021.

He, Y., Wang, K. C., Zhou, C. L., and Wild, M.: A revisit of global dimming and brightening based on the sunshine duration, Geophys. Res. Lett., 45, 4281-4289, 10.1029/2018gl077424, 2018.

He, Y., Wang, K., Yang, K., Zhou, C., Shao, C., and Yin, C.: Homogenized daily sunshine duration at 2°×2° over China from 1961 to 2022 (v1.0), Github [dataset], https://yanyihe-rad.github.io/files/homog-daily-ssd-China-v1.0.mat, 2024.

Hu, S., Mo, Y., Ding, L., and Wang, Z.: Comparative analysis on the performance of digital

Formatted: Font: (Asian) +Body Asian (等线)

sunshine recorder based on photoelectric principle, Meteorological, Hydrological and Marine Instruments, 4, 23-28, 2019.

Lang, G., An, C., and Yuan, Q.: Comparison and analysis of sunshine duration between DFC1 photoelectric digital sunshine recorder and dark-tube sunshine recorder, Mid-low Latitude Mountain Meteorology, 45, 4, 2021.

Li, Z., Yang, X., and Tang, H.: Evaluation of the hourly ERA5 radiation product and its relationship with aerosols over China, Atmos. Res., 294, 106941, https://doi.org/10.1016/j.atmosres.2023.106941, 2023.

Lu, Z., Yu, S., and Hou, S.: Discussions on measurement uncertainty of sunshine duration by Jordan and Campbell-Stokes sunshine recorders, Heilongjiang Meteorology, 29, 31-32, 2012.

Lu, Z., Zhang, Y., Wang, J., Wang, F., and Zhou, Y.: Comparative analysis of manual and automatic sunlight observation data, Heilongjiang Meteorology, 36, 31-32, 2019.

Lv, W., Chong, W., and Ding, L.: Test and analysis on performance comparison of photoelectric automatic sunshine duration recorder, Journal of Electronic Measurement and Instrument, 29, 928-933, 2015.

Ma, Q., Wang, K. C., He, Y. Y., Su, L. Y., Wu, Q. Z., Liu, H., and Zhang, Y. R.: Homogenized century-long surface incident solar radiation over Japan, Earth Syst. Sci. Data, 14, 463-477, 10.5194/essd-14-463-2022, 2022.

Manara, V., Beltrano, M. C., Brunetti, M., Maugeri, M., Sanchez-Lorenzo, A., Simolo, C., and Sorrenti, S.: Sunshine duration variability and trends in Italy from homogenized instrumental time series (1936-2013), J. Geophys. Res. Atom., 120, 3622-3641, 10.1002/2014jd022560, 2015.

Perreault, L., Bernier, J., Bobée, B., and Parent, E.: Bayesian change-point analysis in hydrometeorological time series. Part 1. The normal model revisited, J. Hydrol., 235, 221-241, 2000.

Pincus, R., Platnick, S., Ackerman, S. A., Hemler, R. S., and Patrick Hofmann, R. J.: Reconciling simulated and observed views of clouds: MODIS, ISCCP, and the limits of instrument simulators, J. Clim., 25, 4699-4720, 2012.

Press, W. H., Teukolsky, S. A., Vetterling, W. T., and Flannery, B. P.: Numerical recipes in Fortran 77: the art of scientific computing, Cambridge university press Cambridge 1992.

Reeves, J., Chen, J., Wang, X. L., Lund, R., and Lu, Q. Q.: A review and comparison of changepoint detection techniques for climate data, J. Appl. Meteorol. Climatol., 46, 900-915, 2007.

Sanchez-Lorenzo, A. and Wild, M.: Decadal variations in estimated surface solar radiation over Switzerland since the late 19th century, Atmos. Chem. Phys., 12, 8635-8644, 10.5194/acp-12-8635-2012, 2012.

Sanchez-Lorenzo, A., Brunetti, M., Calbo, J., and Martin-Vide, J.: Recent spatial and temporal variability and trends of sunshine duration over the Iberian Peninsula from a homogenized data

Formatted: Font: (Asian) +Body Asian (等线)

set, J. Geophys. Res. Atom., 112, 10.1029/2007jd008677, 2007.

Shao, C., Yang, K., Tang, W., He, Y., Jiang, Y., Lu, H., Fu, H., and Zheng, J.: Convolutional neural network-based homogenization for constructing a long-term global surface solar radiation dataset, Renew. Sust. Energ. Rev., 169, 112952, https://doi.org/10.1016/j.rser.2022.112952, 2022.

Solow, A. R.: Testing for climate change: An application of the two-phase regression model, J. Climate Appl. Meteorol., 1401-1405, 1987.

Stanhill, G. and Cohen, S.: Solar radiation changes in the United States during the twentieth century: Evidence from sunshine duration measurements, J. Clim., 18, 1503-1512, 2003.

Swales, D. J., Pincus, R., and Bodas-Salcedo, A.: The cloud feedback model intercomparison project observational simulator package: Version 2, Geosci. Model Dev., 11, 77-81, 2018.

Tang, W., He, J., Qi, J., and Yang, K.: A dense station-based long-term and high-accuracy dataset of daily surface solar radiation in China, Earth Syst. Sci. Data, 15, 4537-4551, 2023.

Wang, K., Dickinson, R. E., Wild, M., and Liang, S.: Atmospheric impacts on climatic variability of surface incident solar radiation, Atmos. Chem. Phys., 12, 9581-9592, 10.5194/acp-12-9581-2012, 2012.

Wang, K., Ma, Q., Li, Z., and Wang, J.: Decadal variability of surface incident solar radiation over China: Observations, satellite retrievals, and reanalyses, J. Geophys. Res. Atmos., 120, 6500-6514, 10.1002/2015jd023420, 2015.

Wang, K., Ma, Q., Wang, X., and Wild, M.: Urban impacts on mean and trend of surface incident solar radiation, Geophys. Res. Lett., 41, 4664-4668, 10.1002/2014gl060201, 2014.

Wang, X. L., Wen, Q. H., and Wu, Y.: Penalized maximal t test for detecting undocumented mean change in climate data series, J. Appl. Meteorol. Climatol., 46, 916-931, 2007.

Wang, X. L. L.: Penalized maximal F test for detecting undocumented mean shift without trend change, J. Atmos. Oceanic Technol., 25, 368-384, 10.1175/2007jtecha982.1, 2008a.

Wang, X. L. L.: Accounting for autocorrelation in detecting mean shifts in climate data series using the penalized maximal t or F test, J. Appl. Meteorol. Clim., 47, 2423-2444, 10.1175/2008jamc1741.1, 2008b.

Wang, X. L. L., Chen, H. F., Wu, Y. H., Feng, Y., and Pu, Q. A.: New Techniques for the Detection and Adjustment of Shifts in Daily Precipitation Data Series, J. Appl. Meteorol. Clim., 49, 2416-2436, 10.1175/2010jamc2376.1, 2010.

Wang, Y., Wild, M., Sanchez-Lorenzo, A., and Manara, V.: Urbanization effect on trends in sunshine duration in China, Ann. Geophys., 35, 839-851, 2017.

Wang, Y., Zhang, G., Sun, G., Liu, S., and Yang, J.: Research survey and development trend of sunshine recorder, Chinese Journal of Scientific Instrument, 41, 1-14, 2020.

Wang, Y., Zhang, G., Sun, G., Liu, S., Xu, D., Yang, S., and Wu, L.: A review on sunshine recorders: Evolution of operation principle and construction, Measurement, 186, 110-138, 2021.

Formatted: Font: (Asian) +Body Asian (等线)

Formatted: Font: (Asian) +Body Asian (等线)

Wild, M.: Global dimming and brightening: A review, J. Geophys. Res. Atom., 114, D00D16, 10.1029/2008jd011470, 2009.

Wild, M.: Enlightening global dimming and brightening, Bull. Am. Meteorol. Soc., 93, 27-37, 2012.

Wild, M., Truessel, B., Ohmura, A., Long, C. N., Koenig-Langlo, G., Dutton, E. G., and Tsvetkov, A.: Global dimming and brightening: an update beyond 2000, J. Geophys. Res. Atom., 114, D00D13, 10.1029/2008jd011382, 2009.

Wild, M., Gilgen, H., Roesch, A., Ohmura, A., Long, C. N., Dutton, E. G., Forgan, B., Kallis, A., Russak, V., and Tsvetkov, A.: From dimming to brightening: decadal changes in solar radiation at Earth's surface, Science, 308, 847-850, 10.1126/science.1103215, 2005.

WMO: Guide to Meteorological Instruments and Methods of Observation. WMO-No. 8, Secretariat of the WMO, Geneva, 2014.

Xia, X.: Spatiotemporal changes in sunshine duration and cloud amount as well as their relationship in China during 1954–2005, J. Geophys. Res. D Atmos., 115, 2010.

Yang, S., Wang, X. L., and Wild, M.: Homogenization and trend analysis of the 1958-2016 in situ surface solar radiation records in China, J. Clim., 31, 4529-4541, 10.1175/jcli-d-17-0891.1, 2018.

Yang, S., Shi, G., Wang, B., Yang, H., and Duan, Y.: Trends in Surface Solar Radiation (SSR) and the Effect of Clouds on SSR during 1961-2009 in China, Chinese Journal of Atmospheric Sciences, 37, 963-970, 2013.

Zhao, D., Luo, Y., Gao, G., Zhu, C., and Shen, Y.: Long-Term Changes and Essential Climatic Characteristics of Sunshine Duration over China during 1961-2007, Resources Science, 32, 701-711, 2010.

Zhou, C., He, Y., and Wang, K.: On the suitability of current atmospheric reanalyses for regional warming studies over China, Atmos. Chem. Phys., 18, 8113-8136, 10.5194/acp-18-8113-2018, 2018.

Zhou, C., Wang, K., and Ma, Q.: Evaluation of eight current reanalyses in simulating land surface temperature from 1979 to 2003 in China, J. Clim., 30, 7379-7398, 10.1175/jcli-d-16-0903.1, 2017.

Zhou, C., Wang, J., Dai, A., and Thorne, P.: A New Approach to Homogenize Global Subdaily Radiosonde Temperature Data from 1958 to 2018, J. Clim., 34, 1163-1183, 10.1175/jcli-d-20-0352.1, 2021a.

Zhou, C., Azorin-Molina, C., Engström, E., Minola, L., Wern, L., Hellström, S., Lönn, J., and Chen, D.: HomogWS-se: a century-long homogenized dataset of near-surface wind speed observations since 1925 rescued in Sweden, Earth Syst. Sci. Data, 14, 2167-2177, 2022.

Zhou, H., Quan, W., Wang, Z., Li, X., Li, Y., and Zhao, H.: Comparison of sunshine duration measurements between a Jordan sunshine recorder and three automatic sensors at Shangdianzi GAW station, J. Meteorol. Res., 35, 716-728, 2021b.

Formatted: Font: (Asian) +Body Asian (等线)

677 **Table 1** Trends of sunshine duration (unit: hours·day^{-1}/decade) before and after
678 homogenization in China and its seven subregions, i.e., Northwest China (I), Tibetan Plateau
679 (II), Southwest China (III), Northeast China (IV), North China (V), Southeast China (VI), and
680 Loess Plateau (VII), during three periods of 1961-1990, 1991-2022, and 2013-2022. Trends
681 with a significance level of 0.05 are shown in bold, while those with a significance level of 0.1
682 are italicized.

	1961-1990		1991-2022		2013-2022	
	Before	After	Before	After	Before	After
China	**-0.13**	**-0.11**	*-0.04*	*-0.04*	-0.02	0.07
Northwest China (I)	-0.04	-0.02	-0.06	-0.03	**-0.52**	-0.16
Tibet Plateau (II)	*0.05*	0.02	*-0.05*	**-0.07**	-0.20	*-0.36*
Southwest China (III)	**-0.13**	**-0.11**	*0.06*	0.02	-0.05	-0.16
Northeast China (IV)	**-0.11**	**-0.10**	-0.01	-0.02	0.23	0.26
North China (V)	**-0.22**	**-0.18**	**-0.14**	**-0.12**	0.16	*0.42*
Southeast China (VI)	**-0.23**	**-0.21**	-0.02	-0.02	0.10	0.21
Loess Plateau (VII)	*-0.13*	-0.11	**-0.11**	-0.08	-0.08	0.11

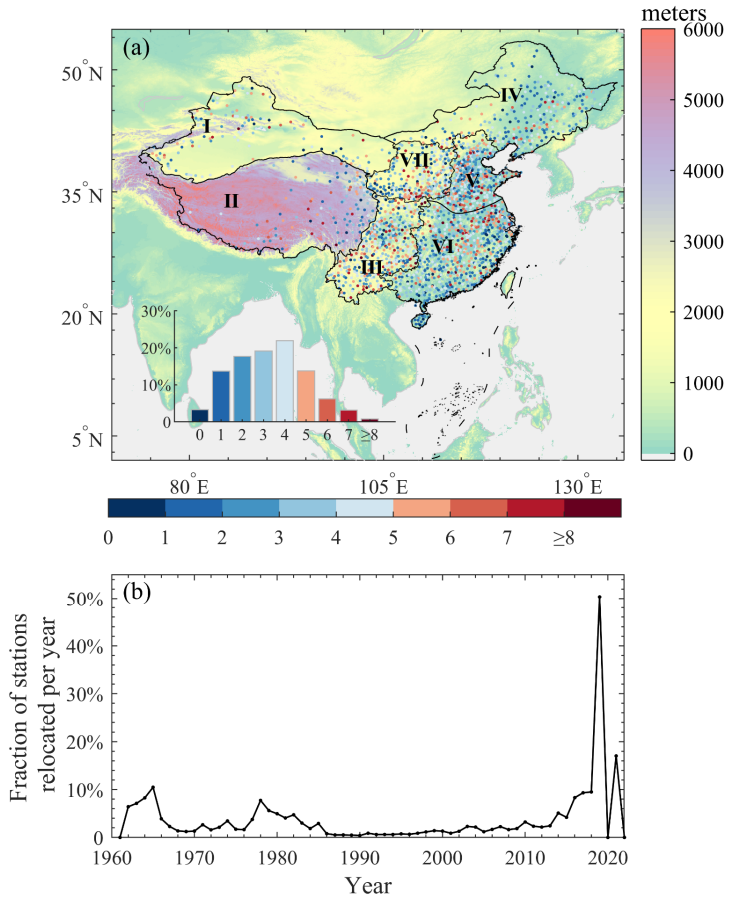

683

684 **Figure 1** (a) Map of the number of relocations for 2,263 national meteorological stations (dots
685 colored by the bottom color bar, unit: times) in China during the period of 1961 to 2022. A
686 relocation event is defined as Δlatitude > 0.01°, Δlongitude > 0.01°, or Δaltitude > 10m before
687 and after a specific date. The elevation map serves as the background and is colored by the
688 right-side color bar. The sub-figure in the bottom left illustrates the percentage of stations
689 corresponding to the number of relocations for all stations. According to topography and
690 administrative divisions of China, seven subregions were identified, i.e., Northwest China (I),
691 Tibetan Plateau (II), Southwest China (III), Northeast China (IV), North China (V), Southeast
692 China (VI), and Loess Plateau (VII). (b) Time series of the fraction of stations (unit: %) that
693 underwent one or more relocations per year. The unusually frequent relocations in 2019 were
694 accompanied with the instrument replacements that occurred that year.

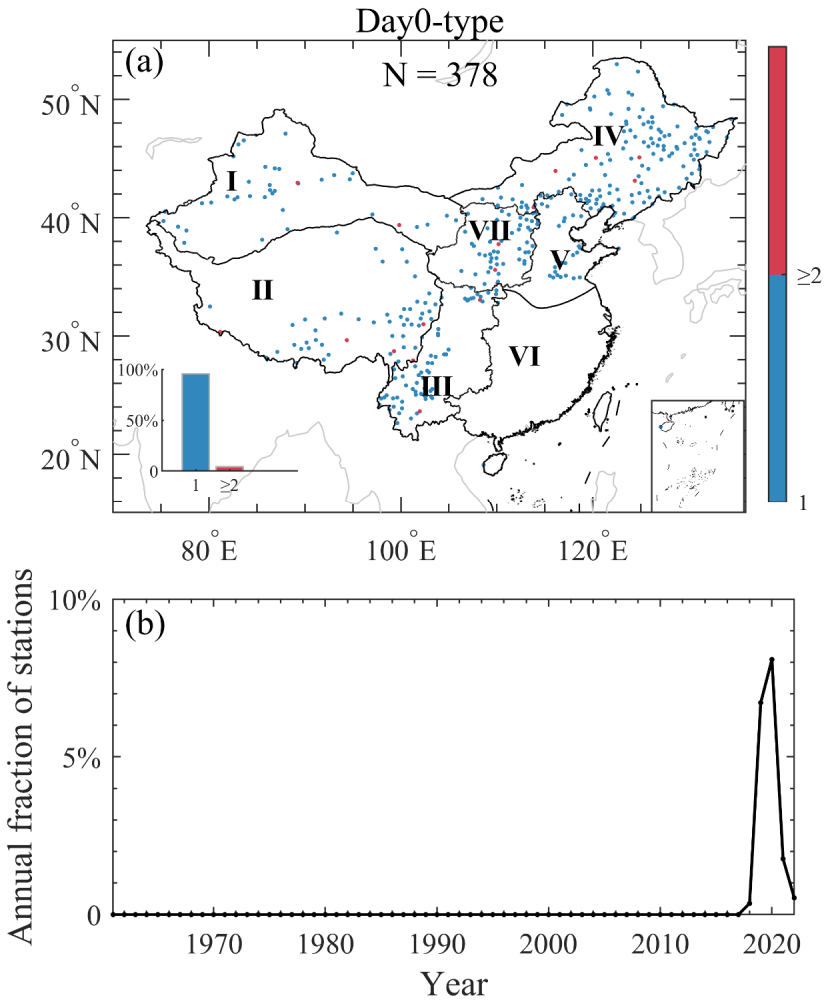

695

696 **Figure 2** (a) Map of stations with the day0-type discontinuities in the monthly count of days
697 with zero sunshine duration. The right-side color bar illustrates the total number of segments
698 with the day0-type discontinuities for each station. The sub-figure in the bottom left shows the
699 percentage of stations with different numbers of such segments per station. A total of 378
700 stations were identified with the day0-type discontinuities. (b) Annual fraction (unit: %) of
701 stations with the day0-type discontinuities from 1961 to 2022.

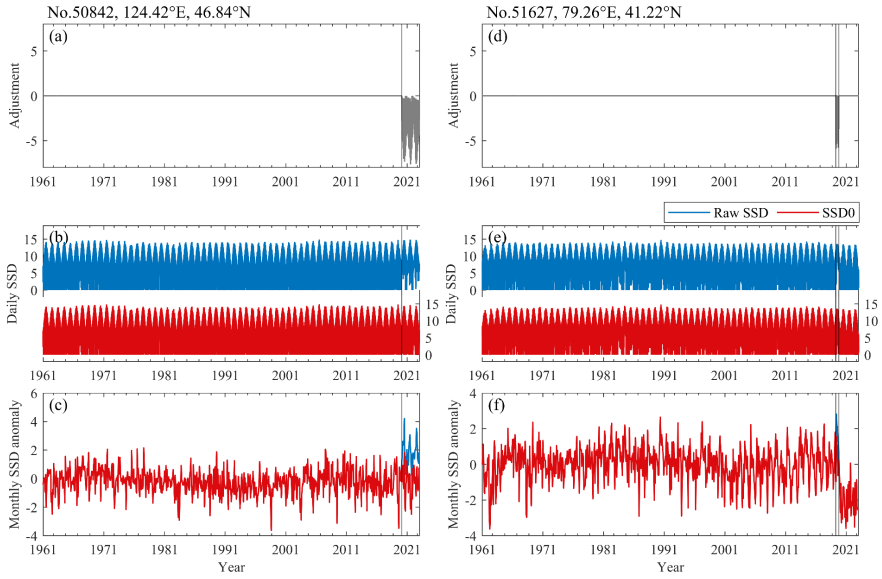

Figure 3 Comparison of raw sunshine duration (Raw SSD, blue line, unit: hours·day^{-1}) with the day0-type corrected sunshine duration (SSD0, red line, unit: hours·day^{-1}) at two example stations in (a-c) Northeast China and (d-f) Northwest China, respectively. (a and d) QM adjustments added to the raw SSD; (b and e) Daily time series of the raw SSD and SSD0; (c and f) as in (b and e), but for their monthly SSD anomalies. The vertical grey lines indicate the start and end dates of segments identified with the day0-type discontinuities.

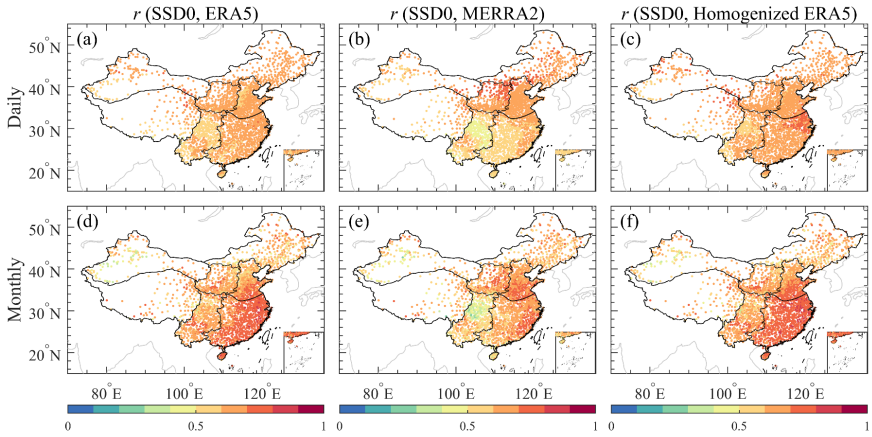

709

710 **Figure 4** Maps of the correlation coefficients of sunshine duration at daily, monthly and annual
711 time scales between the day0-type corrected observation (SSD0) and ERA5, MERRA2 as well
712 as homogenized ERA5.

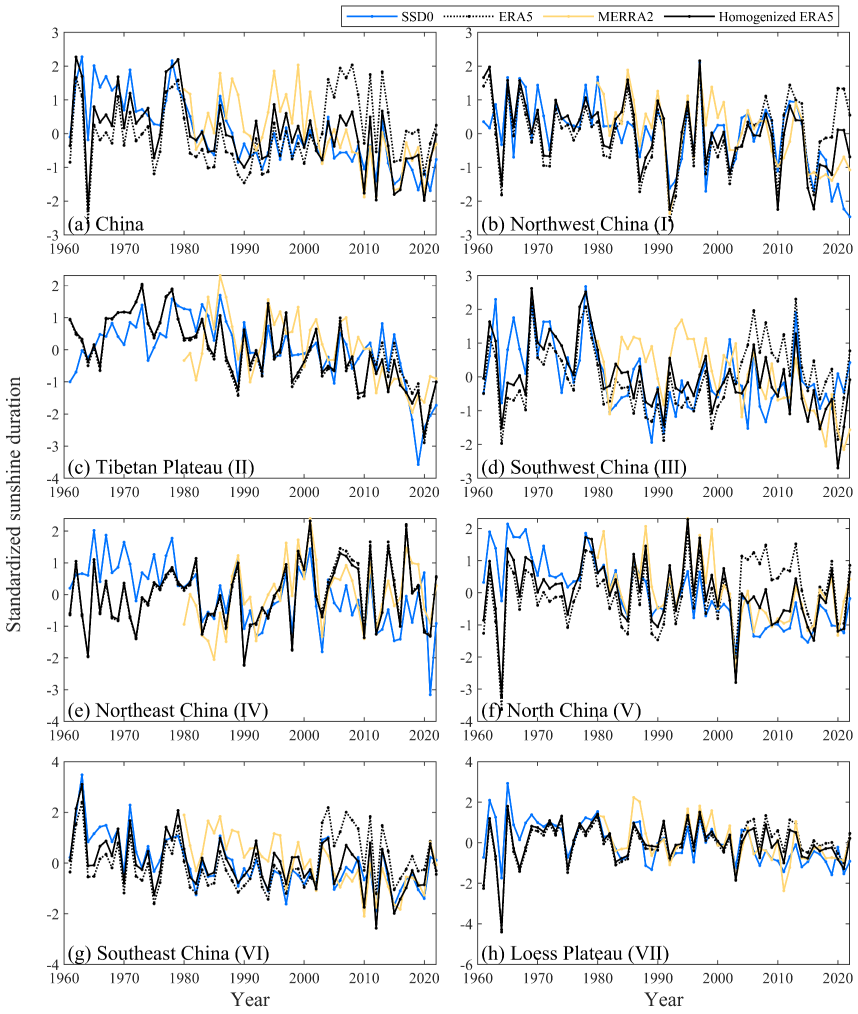

713

714 **Figure 5** Time series of the standardized sunshine duration (unit: 1) from the day0-type
715 corrected observation (SSD0, blue line), ERA5 (black-dotted line), MERRA2 (yellow line),
716 and homogenized ERA5 (black line) in (a) China and (b-h) its seven subregions.

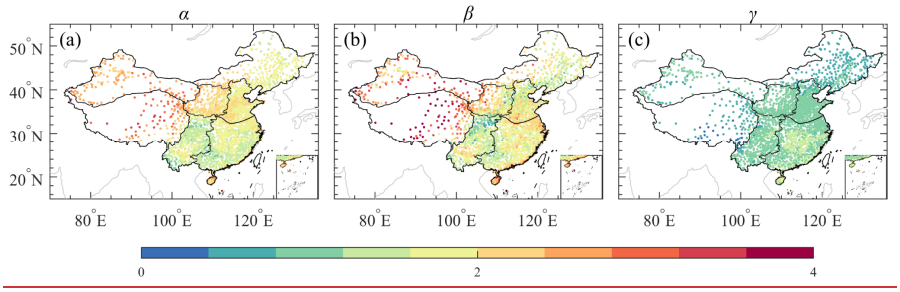

Figure 6 (a) Map of the linear regression coefficient (α) of the daily anomalies of $SSDd_{obs}$ against $SSDd_{ERA5}$. (b-c) Same as (a), but showing β for $SSDm_{obs}$ against $SSDm_{ERA5}$, and γ for $SSDd_{obs}$ against $SSDd_{ERA5}$, respectively. For more details, refer to Equations 1, 4, and 5.

Formatted: Font: Bold

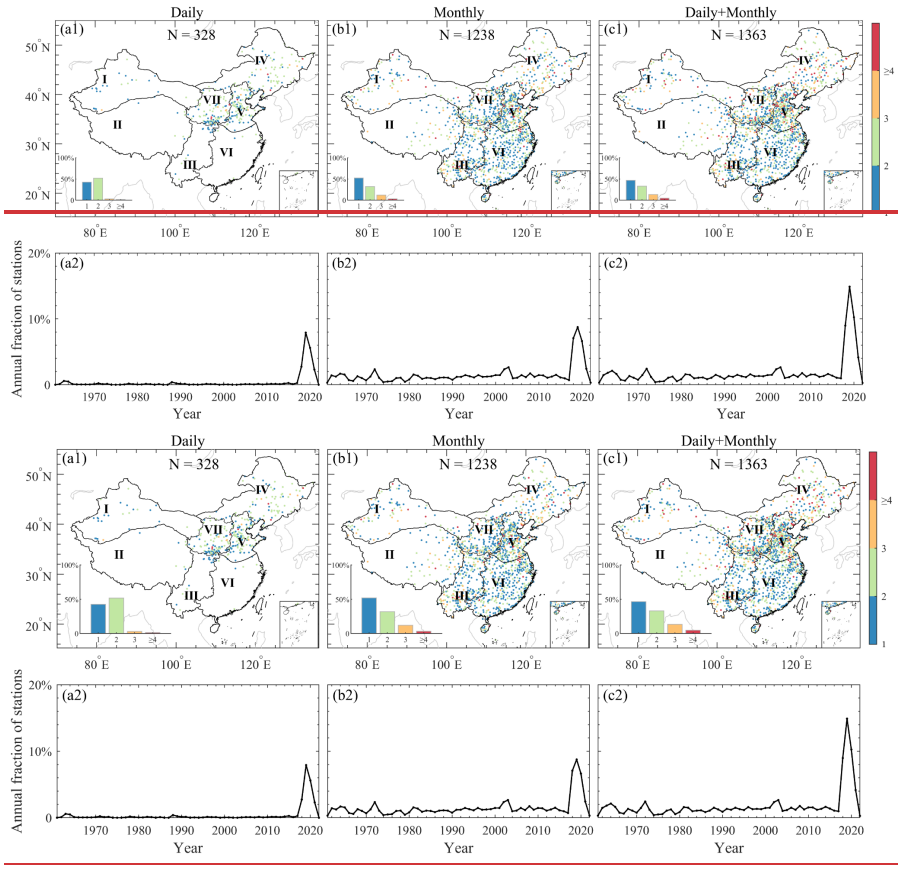

721

722

723 **Figure** ~~6~~7 (a1 and b1) Maps of the number of breakpoints detected in the daily variance and
724 monthly mean of the non-zero SSD0 series, respectively. (c1) Map of the number of
725 breakpoints merged from those in Figure 7~~6~~a1 and 7~~6~~b1. The total number (N) of stations with
726 one or more breakpoints from 1961 to 2022 is shown in each panel. (a2, b2, and c2) Annual
727 fraction (unit: %) of stations with the breakpoints from 1961 to 2022.

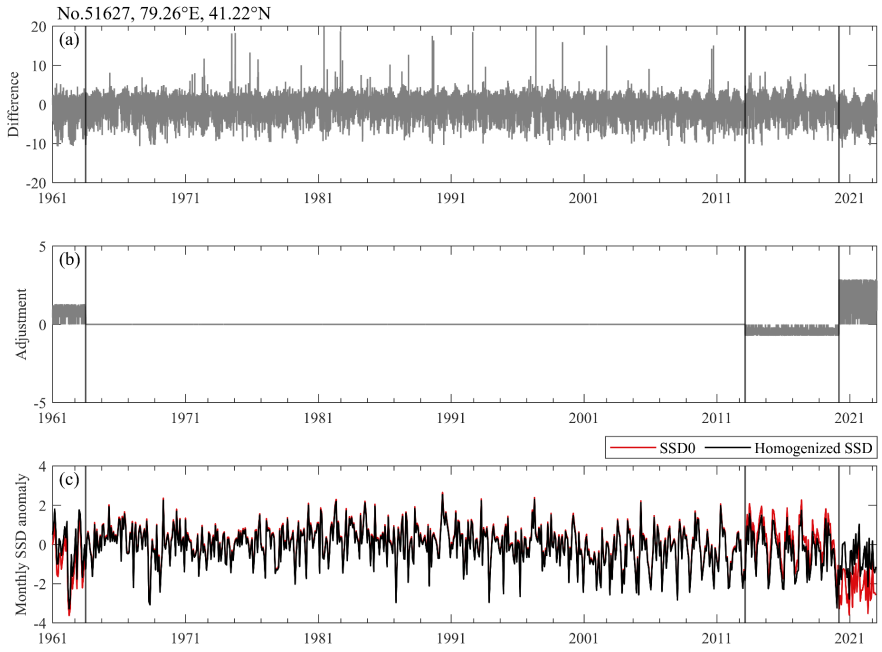

Figure 8~~7~~ Comparison of the day0-type corrected sunshine duration (SSD0, red line) before and after homogenization (Homogenized SSD, black line) at an example Station No. 51627 in Northwest China. (a) Daily SSD difference (unit: hours·day^{-1}) between the SSD0 and the corrected ERA5 reference series; (b) QM adjustments added to the SSD0; (c) Monthly anomaly series of the SSD0 (red line) and homogenized data (black line). The vertical lines indicate the dates of the breakpoints detected.

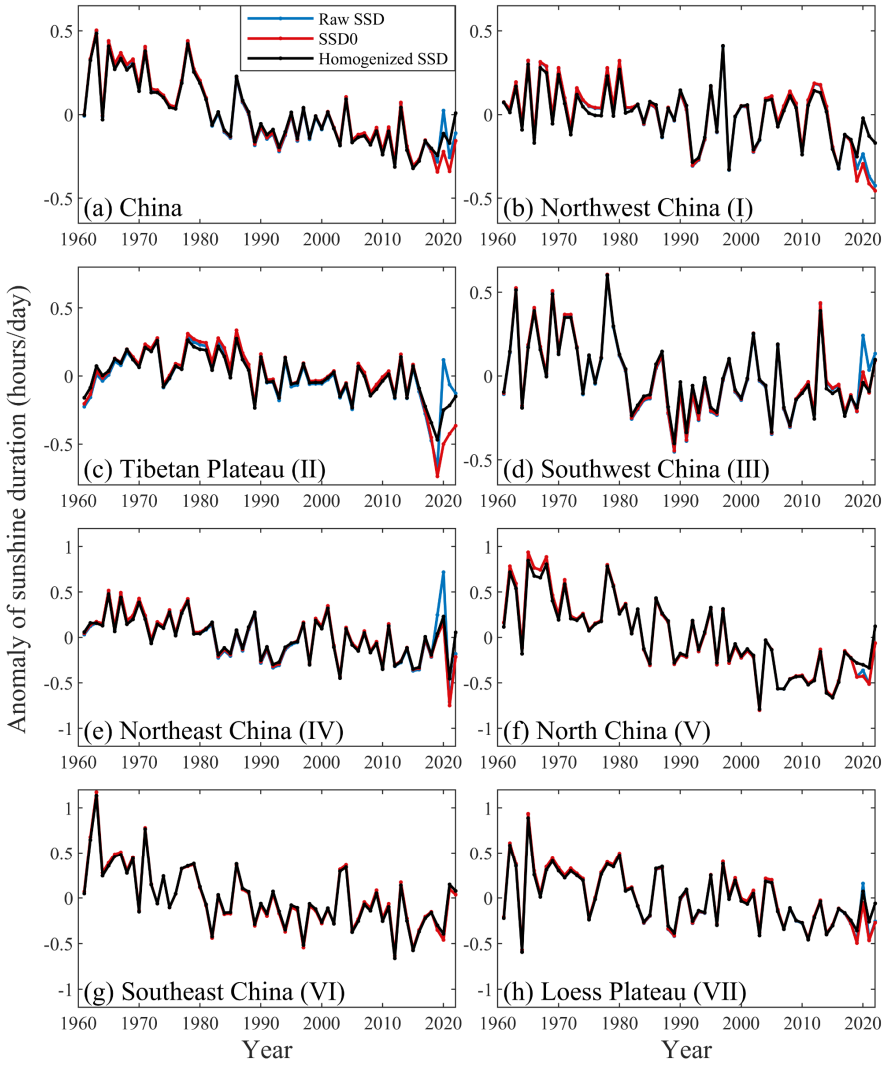

735

736 **Figure ~~8~~9** Time series of raw sunshine duration (Raw SSD, blue line), the day0-type corrected
737 SSD0 (red line), and the homogenized SSD (black line) in (a) China and (b-h) its seven
738 subregions from 1961 to 2022. The anomaly is referenced to the average for the entire period.

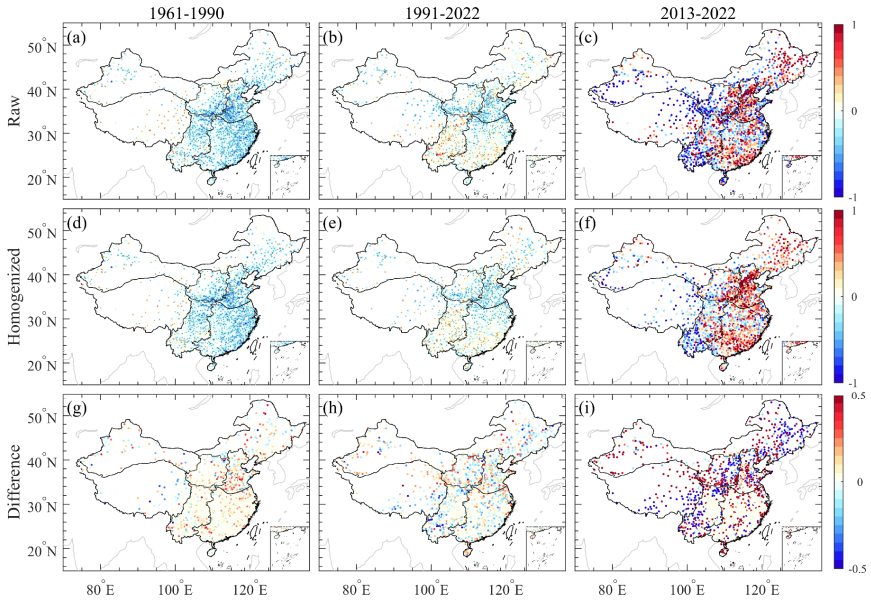

739

740 **Figure 10~~9~~** Maps of the decadal changes (unit: hours·day^{-1}/decade) in (a-c) raw sunshine
741 duration, (d-f) homogenized SSD, and (g-i) their difference over China during three periods of
742 1961-1990, 1991-2022, and 2013-2022, respectively. Black dots superimposed on the colored
743 circles indicate a significance level of 0.10.

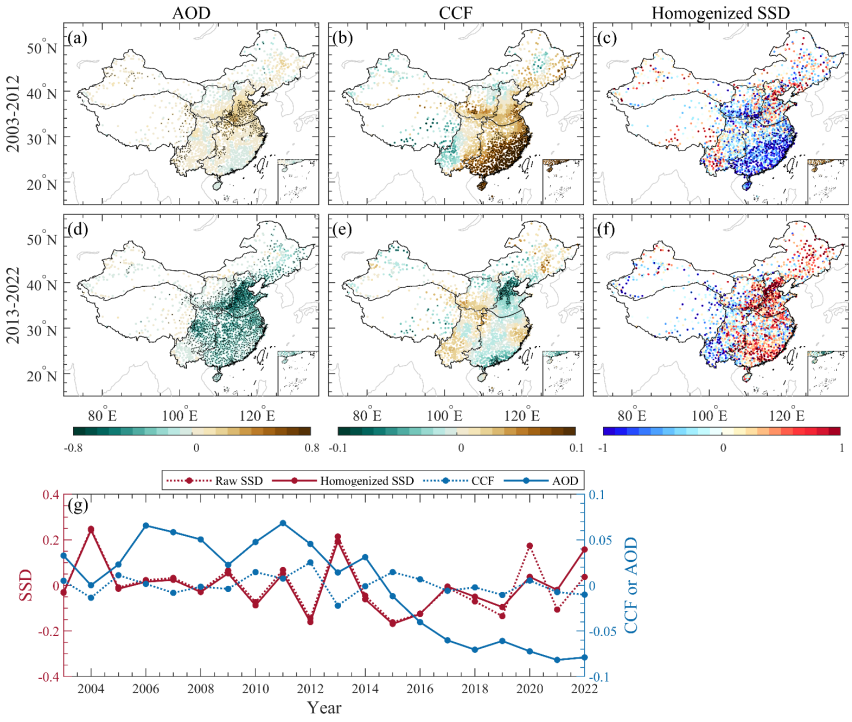

744

745 **Figure 1~~0~~** (a-c) Maps of the decadal changes in aerosol optical depth (AOD, unit: 1/decade),
746 cloud cover fraction (CCF, unit: 1/decade), and homogenized sunshine duration (Homogenized
747 SSD, unit: hours·day^{-1}/decade) over China from 2003 to 2012. (d-f) Same as Figure 1~~0~~a-1~~0~~c,
748 but from 2013 to 2022. Black dots indicate a significance level of 0.10. (g) Time series of the
749 raw SSD (red dotted line), homogenized SSD (red solid line), CCF (blue dotted line) and AOD
750 (blue solid line) from 2003 to 2022.